

# Antiferromagnetic to superconducting phase transition in the hole- and electron-doped Hubbard model at zero temperature

M. Aichhorn,<sup>1</sup> E. Arrighoni,<sup>2</sup> M. Potthoff,<sup>1</sup> and W. Hanke<sup>1</sup>

<sup>1</sup>*Institute for Theoretical Physics, University of Würzburg, Am Hubland, 97074 Würzburg, Germany*

<sup>2</sup>*Institute for Theoretical Physics and Computational Physics, Graz University of Technology, Petersgasse 16, 8010 Graz, Austria*

(Received 14 December 2005; revised manuscript received 1 June 2006; published 13 July 2006)

The competition between  $d$ -wave superconductivity (SC) and antiferromagnetism (AF) in the high- $T_c$  cuprates is investigated by studying the hole- and electron-doped two-dimensional Hubbard model with a recently proposed variational quantum-cluster theory. The approach is shown to provide a thermodynamically consistent determination of the particle number, provided that an overall shift of the on-site energies is treated as a variational parameter. The consequences for the single-particle excitation spectra and for the phase diagram are explored. By comparing the single-particle spectra with quantum Monte Carlo and experimental data, we verify that the low-energy excitations in a strongly correlated electronic system are described appropriately. The cluster calculations also reproduce the overall ground-state phase diagram of the high-temperature superconductors. In particular, they include salient features such as the enhanced robustness of the antiferromagnetic state as a function of electron doping and the tendency towards phase separation into a mixed antiferromagnetic-superconducting phase at low doping and a pure superconducting phase at high (both hole and electron) doping.

DOI: [10.1103/PhysRevB.74.024508](https://doi.org/10.1103/PhysRevB.74.024508)

PACS number(s): 74.20.-z, 71.10.-w, 75.10.-b

## I. INTRODUCTION

The theory of high-temperature superconductivity remains one of the most challenging problems in solid-state physics. In many metallic compounds, over a broad range of compositions and temperatures, only two phases are encountered: i.e., the normal (Fermi liquid) and a magnetic or superconducting phase. In sharp contrast, the high-temperature superconductors (HTSC's) and other strongly correlated electron systems, such as heavy-fermion and a variety of transition-metal oxide systems, exhibit many ordered phases, which appear to compete and sometimes coexist.<sup>1</sup> In the HTSC's, besides ordered antiferromagnetic (AF) and superconducting (SC) phases, compelling evidence exists for charge- and spin-“stripe” phases and phases with coexisting SC and AF order.<sup>2</sup> The common denominator and the underlying reason for these competing orders is certainly the presence of strong electronic correlations and Mott-Hubbard physics: The interplay between kinetic-energy and Coulomb-correlation effects induces an extreme sensitivity to external parameters (doping, temperature, pressure, etc.) and a rather difficult to predict “outcome”: i.e., the characteristic low-energy excitations and the phase diagram at low temperatures. The central challenge in the field of high- $T_c$  superconductivity is, therefore, the connection of the (known) microscopic interactions at the level of electrons and ions, which are at high energy ( $\sim eV$ ) and temperature  $T$ , with the “emerging phenomena” at  $T=0$ : i.e., competing and nearly degenerate orders. Ideally, one should employ a systematic renormalization-group approach to integrate out the irrelevant degrees of freedom and, thereby, correctly bridge high to low energies and eventually go to  $T=0$ . It is, however, by no means obvious how to do this when strong correlations are present, such as in the HTSC's.

In this context cluster techniques, which systematically approach the infinite-size (low-energy) limit, provide a pow-

erful alternative.<sup>3-5</sup> In this paper, we will discuss and apply a variational-cluster approach (VCA) which was proposed recently.<sup>6,7</sup> It is based on the self-energy-functional theory (SFT),<sup>8</sup> which provides a general variational scheme to use dynamical information from an exactly solvable “reference system” (in our case, an isolated cluster) to go to the infinite-size lattice fermion problem at low temperatures and at  $T=0$ , in particular. In our earlier work<sup>7</sup> this scheme was formulated to study phases with spontaneously broken symmetry. For the cluster sizes used, it was shown that the VCA correctly reproduces long-range AF order for the two-dimensional (2D) Hubbard model and the absence of this order in one dimension. This nontrivial “test” implies that the VCA goes well beyond ordinary mean-field theory.

Another crucial test is provided by the dynamical information contained in the one-particle Green's function  $\mathbf{G}$ . Compared to variational schemes based on wave functions,<sup>9</sup> an important advantage of the VCA consists in the fact that it quite naturally gives the one-electron Green's function  $\mathbf{G}$ . For the 2D Hubbard model, it was recently demonstrated<sup>7</sup> that the VCA, with the lattice tiled by  $(\sqrt{10} \times \sqrt{10})$  clusters, correctly reproduces low-temperature quantum Monte Carlo (QMC) data—in particular, the coherent and incoherent “bands” experimentally known from angle-resolved photoemission spectroscopy (ARPES) data.<sup>10</sup>

These tests provide also the foundation for attacking the question whether the “minimal” microscopic model—namely the 2D one-band Hubbard model—reproduces the essential features of the electron- and hole-doped HTSC phase diagram. We will not go into a lengthy discussion of what interactions should be retained at the electron-ion level. But when choosing the 2D one-band Hubbard model<sup>11</sup>—i.e.,

$$H = \sum_{ij\sigma} t_{ij} c_{i\sigma}^\dagger c_{j\sigma} + U \sum_i n_{i\uparrow} n_{i\downarrow}, \quad (1)$$

where  $c_{j\sigma}$  and  $c_{i\sigma}^\dagger$  are the usual annihilation and creation operators,  $t_{ij}$  denote the hopping-matrix elements,  $n_{i\sigma}$

$=c_{i\sigma}^\dagger c_{i\sigma}$  is the density at site  $i$  with spin  $\sigma = \uparrow, \downarrow$ , and  $U$  is the local Coulomb repulsion, one has introduced gross simplifications, leaving out other orbital (e.g.,  $p$ ) degrees of freedom, long-range Coulomb interaction, electron-phonon coupling, etc. Nevertheless, this choice appears to be legitimate, last but not least in view of the amazing agreement achieved between numerical simulations and experimental results for the normal-state properties of the cuprates (see, for example, Refs. 1 and 11–13).

The ground-state phase diagram of the model was recently investigated using the VCA by S en echal *et al.*<sup>14</sup> and by two of us.<sup>15</sup> There are important technical differences, but the “upshot” of the two works is as follows: For the cluster sizes used in the VCA, the  $T=0$  phase diagram of the Hubbard model (including hopping terms up to second- or third-nearest neighbors) turns out to be qualitatively similar to that of the electron- and hole-doped cuprates. The model correctly describes the overall phase diagram, such as the occurrence of the AF and SC phases, and predicts the corresponding doping ranges in qualitative agreement with the experiments for the cuprate materials.

The present paper has several purposes: First, we would like to stress that for an application of the VCA to the high- $T_c$  problem it is of crucial importance to treat the on-site energies in the reference system as variational parameters. We will show that this ensures a thermodynamically consistent determination of the average particle number. Compared to the study of Ref. 14 this represents an important methodical extension. On the other hand, without the variational optimization of the on-site energy, one has to tolerate an inconsistency in the determination of the average particle number. The effects of this error shall be demonstrated by model calculations. The issue of thermodynamic consistency is also discussed for the off-diagonal elements of the one-particle density matrix and, in case of spontaneous symmetry breaking, for the respective order parameter. It is interesting to note that there are no such problems in the dynamical mean-field theory<sup>16,17</sup> (DMFT) and its cluster extensions.<sup>18,19</sup> Here the on-site energies are kept at their “physical” values from the very beginning rather than being determined from the self-consistency condition. The (cellular) DMFT, however, can be considered as a special approximation within the general SFT framework.<sup>6,7</sup> Hence, the question arises as to why a fixed on-site energy does *not* spoil thermodynamic consistency in the case of (cellular) DMFT. It is interesting to note that, in the case of interacting bosons, the issue of consistency has also been shown to be very important, recently.<sup>20</sup>

Second, an accurate analysis of the behavior of the chemical potential as a function of the particle density close to the transition to a nonmagnetic state, as well as a corresponding Maxwell construction, indicates the presence of an inhomogeneous ground state with macroscopically large regions of low- and high-particle density. Using  $L_c=4$ -site clusters, we can get a rough estimate of the ground-state phase diagram and investigate the instability of the homogeneous (AF, SC) phases against charge inhomogeneities. This represents an important complement to the work of Ref. 14, where larger cluster sizes up to  $L_c=10$  sites have been considered but without an appropriate analysis via a Maxwell construction.

Finally, our numerical results give valuable insights into different questions of the high- $T_c$  problem, as they provide

direct access to the single-particle excitation spectrum in the strong-coupling regime at zero temperature. This has to be contrasted with the work of Maier *et al.*<sup>21,22</sup> who have been able to treat clusters with  $L_c > 20$  sites within the dynamical cluster approximation (DCA), but are restricted to finite temperatures, intermediate coupling  $U/t \lesssim 4$ , and imaginary time. A review comparing the application of different cluster (SFT, DCA, and cellular DMFT) as well as weak-coupling methods for the Hubbard model has appeared recently.<sup>4</sup>

Our paper is organized as follows: We start with a summary of the central ideas of the SFT in general (Sec. II A). Thermodynamic consistency with respect to the average particle number is discussed in Sec. II B. Consistency with respect to the off-diagonal elements of the density matrix is addressed in Appendix AA and the case of the C-DMFT is discussed in Appendix B. Our theoretical considerations are completed by describing some computational details of the VCA calculations in Sec. II C. Section III then presents the results for the  $T=0$  spectral function  $A(\mathbf{k}, \omega)$  for electron and hole doping. We discuss how the characteristically different doping dependences of the spectra give rise to different Fermi-surface evolutions upon doping. These Fermi-surface evolutions can then be tied up with the characteristic differences in the electron- and hole-doped phase diagrams, such as the enhanced robustness of the AF order in the electron-doped case. The ground-state phase diagram will be presented and discussed in detail in Sec. IV. Finally, Sec. V contains our main conclusions and a summary.

## II. THEORETICAL BACKGROUND

### A. Self-energy-functional theory

The central idea of the self-energy-functional theory<sup>8</sup> is to make use of the universality of the Luttinger-Ward functional  $\Phi_U[\mathbf{G}]$  (Ref. 23) or of its Legendre transform  $F_U[\mathbf{\Sigma}]$ : For a system with Hamiltonian  $H=H_0(t)+H_1(U)$ , where  $t$  are the one-particle and  $U$  the interaction parameters, the functional dependence  $\Phi_U[\dots]$  or  $F_U[\dots]$  is independent of  $t$ . This universality is obvious as the Luttinger-Ward functional is defined via a skeleton-diagram expansion involving dressed propagators and vertices only.<sup>23</sup>

Concentrating on the self-energy  $\mathbf{\Sigma}$  instead of the single-particle Green’s function  $\mathbf{G}$ , the grand potential of the system at temperature  $T$  and chemical potential  $\mu$  can be written as a functional of  $\mathbf{\Sigma}$ :

$$\Omega_{t,U}[\mathbf{\Sigma}] = \text{Tr} \ln(\mathbf{G}_{0,t}^{-1} - \mathbf{\Sigma})^{-1} + F_U[\mathbf{\Sigma}], \quad (2)$$

where  $\mathbf{G}_{0,t} = (\omega + \mu - t)^{-1}$  is the free Green’s function and  $\text{Tr} \equiv T \sum_{\omega_n} e^{i\omega_n 0^+} \text{tr}$  with the usual trace  $\text{tr}$  and the Matsubara frequencies  $\omega_n = (2n+1)\pi T$  for integer  $n$ . At the physical self-energy  $\mathbf{\Sigma} = \mathbf{\Sigma}_{t,U}$ , the grand potential is stationary:  $\delta\Omega_{t,U}[\mathbf{\Sigma}_{t,U}] = 0$ .

Why is it more advantageous to express  $\Omega$  as a functional of the self-energy  $\mathbf{\Sigma}$  rather than  $\mathbf{G}$ ? This has to do with the “short-range” character of  $\mathbf{\Sigma}$  as a function of its real-space coordinates,<sup>24</sup> which in general is due to the fact that  $\mathbf{\Sigma}$  is qualitatively related to a dynamically screened particle-particle interaction. For the Hubbard model, in particular,

one believes that important effects are sufficiently accounted for by a local<sup>25</sup> or short-ranged<sup>26</sup> self-energy, at least for high lattice dimensions. A local or short-ranged self-energy, however, can be well generated by a cluster of finite size, and for the subsequent optimization of the cluster trial self-energy, the self-energy functional (2) can be used. This concept allows for the construction of a class of conceptually clear and thermodynamically consistent approximations, including the dynamical mean-field theory<sup>16,17</sup> and a cluster extension of the DMFT (Ref. 18) (see Ref. 27 for a detailed discussion).

Due to the universality of  $F_U[\Sigma]$ , we have

$$\Omega_{t',U}[\Sigma] = F_U[\Sigma] + \text{Tr} \ln(\mathbf{G}_{0,t'}^{-1} - \Sigma)^{-1} \quad (3)$$

for the self-energy functional of a so-called ‘‘reference system,’’ which is given by a Hamiltonian with the same interaction part  $U$  but modified one-particle parameters  $t'$ :  $H' = H_0(t') + H_1(U)$ . Although it has different microscopic parameters, the reference system is assumed to be in the same macroscopic state as the original system, so it has the same temperature  $T$  and the same chemical potential  $\mu$ . By a proper choice of its one-particle part, the problem posed by the reference system  $H'$  can be much simpler than the original problem posed by  $H$ , such that the self-energy of the reference system,  $\Sigma_{t',U}$ , can be computed exactly within a certain subspace of parameters  $t'$ . Combining Eqs. (2) and (3), we can eliminate the functional  $F_U[\Sigma]$ . Inserting as a trial self-energy the self-energy of the reference system then yields

$$\Omega_{t,U}[\Sigma_{t',U}] = \Omega_{t',U} + \text{Tr} \ln(\mathbf{G}_{0,t}^{-1} - \Sigma_{t',U})^{-1} - \text{Tr} \ln \mathbf{G}_{t',U}, \quad (4)$$

where  $\Omega_{t',U}$  and  $\mathbf{G}_{t',U}$  are the grand potential and the Green's function of the reference system. Stationary points are obtained, and this is the approximation, by restricting the variation to the subspace of trial self-energies  $\Sigma_{t',U}$ :

$$\frac{\partial \Omega_{t,U}[\Sigma_{t',U}]}{\partial t'} = 0 \quad \text{for } t' = t'_s. \quad (5)$$

Varying the trial self-energy means to vary the one-particle parameters  $t'$  of the reference system. For further details of the approach see Ref. 8.

Here, we will focus on the Hubbard model, Eq. (1), as the original model given by  $H$ . Different possible choices for  $H'$  and the corresponding systematics of approximations generated in this way are discussed in Ref. 27. In the following, we will concentrate on two cluster approaches: (i) the variational cluster approach<sup>6,7</sup> and (ii) the cellular DMFT (C-DMFT).<sup>18</sup> The VCA can be seen as a variational generalization of the cluster-perturbation theory.<sup>28,29</sup> It is obtained by partitioning the infinite lattice into disconnected (identical) clusters of  $L_c$  sites each and choosing  $H'$  to consist of the intracluster parts only; i.e., the intercluster hopping is switched off in  $H'$ . The C-DMFT is a cluster variant of the DMFT. In the context of the SFT, it is obtained in the same way as the VCA but with an additional coupling of each of the  $L_c$  correlated cluster sites to a continuous bath—i.e., to an infinite number of uncorrelated additional bath sites. The on-

site energies of the bath sites as well as their coupling to the original sites are treated as variational parameters.

### B. Consistent determination of the particle density

Once a reference system is specified, one should, in principle, vary *all* one-particle parameters of  $H'$ . This procedure would give the optimal result but requires a search for a stationary point in a high-dimensional parameter space. From a pragmatic point of view it is thus advisable to concentrate on a few parameters only which have to be selected by physical arguments. Here, we argue that the variation of the on-site energies is important to achieve thermodynamic consistency with respect to the average particle number. In the case of the Hubbard model, this means to consider the site-independent energy  $\varepsilon' \equiv t'_{ii}$  as (one of the) variational parameter(s).

The average particle number  $\langle N \rangle$  can be calculated in two different ways: on the ‘‘zero-particle level’’ by differentiation of the grand potential with respect to the chemical potential  $\mu$ ,

$$\langle N \rangle = - \frac{\partial \Omega}{\partial \mu}, \quad (6)$$

and on the ‘‘one-particle level’’ by frequency integration of the one-particle excitation spectrum:

$$\langle N \rangle = \sum_{i\sigma} \langle n_{i\sigma} \rangle = \sum_{i\sigma} \int_{-\infty}^{\infty} f(\omega) A_{ii\sigma}(\omega) d\omega. \quad (7)$$

Here,  $A_{ii\sigma}(\omega) = -\text{Im} G_{ii\sigma}(\omega + i0^+)/\pi$  is the local (possibly spin-dependent) spectral density with  $\mathbf{G} = \mathbf{G}_{t,U}$  for short, and  $f(\omega) = [\exp(\omega/T) + 1]^{-1}$  is the Fermi function. For simplicity, we exclude noncollinear magnetic states and assume all expectation values to be diagonal in the spin index.

Thermodynamic consistency means that both ways of calculating  $\langle N \rangle$  yield the same result. Since  $\Omega \equiv \Omega_{t,U}[\Sigma_{t'_s,U}]$  is the *approximate* SFT grand potential at the stationary point  $t' = t'_s$ , and since the spectral density or, equivalently, the one-particle Green's function is the *approximate* Green's function given by  $\mathbf{G} \equiv 1/(\mathbf{G}_{0,t}^{-1} - \Sigma_{t'_s,U})^{-1}$ , the equivalence of Eqs. (6) and (7) is by no means understood *a priori*.

To prove thermodynamic consistency, we start from Eq. (6). According to Eq. (4), there is a twofold  $\mu$  dependence of  $\Omega = \Omega_{t,U}[\Sigma_{t'_s,U}]$ : (i) an *explicit*  $\mu$  dependence due to the chemical potential in the free Green's function of the original model,  $\mathbf{G}_{0,t}^{-1} = \omega + \mu - t$ , and (ii) an *implicit*  $\mu$  dependence due to the  $\mu$  dependence of the self-energy  $\Sigma_{t'_s,U}$ , the Green's function  $\mathbf{G}_{t'_s,U}$ , and the grand potential  $\Omega_{t'_s,U}$  of the reference system:

$$\langle N \rangle = - \frac{\partial \Omega}{\partial \mu_{\text{ex}}} - \frac{\partial \Omega}{\partial \mu_{\text{im}}}. \quad (8)$$

Note that the implicit  $\mu$  dependence is due to the chemical potential of the reference system which, by construction, is in the same macroscopic state as the original system (with the same temperature  $T$  and the same chemical potential  $\mu$ ) *as well as* due to the  $\mu$  dependence of the stationary point  $t'_s$

itself. This is a subtlety which, however, can be ignored since

$$\frac{\partial \Omega}{\partial t'} \cdot \frac{\partial t'}{\partial \mu} = 0 \quad (9)$$

for  $t' = t'_s$  because of stationarity condition (5). (Actually, only those elements of  $t'_s$  show up a  $\mu$  dependence that are treated as variational parameters. According to the chain rule, however, the derivative of  $\Omega$  has to be performed just with respect to those elements, with a vanishing result due to the stationarity condition.)

The self-energy, the Green's function, and the grand potential of the reference system are defined as grand-canonical averages. Hence, their  $\mu$  dependence due to the grand-canonical Hamiltonian  $\mathcal{H}' = H' - \mu N$  is (apart from the sign) the same as their dependence on  $\varepsilon'$ :  $\partial / \partial \mu_{\text{im}} = -\partial / \partial \varepsilon'$ , etc. Consequently, we have

$$\langle N \rangle = -\frac{\partial \Omega}{\partial \mu_{\text{ex}}} + \frac{\partial \Omega}{\partial \varepsilon'}. \quad (10)$$

The first derivative is readily calculated:

$$\begin{aligned} \frac{\partial \Omega}{\partial \mu_{\text{ex}}} &= \frac{\partial}{\partial \mu_{\text{ex}}} T \sum_{\omega_n} e^{i\omega_n 0^+} \text{tr} \ln \frac{1}{\mathbf{G}_{0,t}^{-1}(i\omega_n) - \Sigma_{t',U}(i\omega_n)} \\ &= T \sum_{\omega_n} e^{i\omega_n 0^+} \text{tr} \frac{-1}{i\omega_n + \mu - t - \Sigma_{t',U}(i\omega_n)} \\ &= \frac{-1}{2\pi i} \oint_{\mathcal{C}} e^{\omega 0^+} f(\omega) \text{tr} \frac{-1}{\omega + \mu - t - \Sigma_{t',U}(\omega)} d\omega. \end{aligned} \quad (11)$$

Here, the contour  $\mathcal{C}$  encloses the first-order poles of the Fermi function at  $\omega_n = (2n+1)\pi T$  in a counterclockwise direction. Using Cauchy's theorem, we can proceed to an integration over real frequencies. Inserting into Eq. (10), we get

$$\langle N \rangle = -\frac{1}{\pi} \text{Im} \int_{-\infty}^{\infty} f(\omega) \text{tr} \frac{1}{\mathbf{G}_{0,t}^{-1} - \Sigma_{t',U}} \Big|_{\omega+i0^+} d\omega + \frac{\partial \Omega}{\partial \varepsilon'} \quad (12)$$

for  $t' = t'_s$ .

The first term on the right-hand side is just the expression for the average particle number given by Eq. (7). The second term on the right-hand side vanishes *provided that* the variational condition (5) is satisfied—i.e., *provided that*  $\varepsilon'$  is included in the set of variational parameters. In this case one has thermodynamic consistency. If  $\varepsilon'$  was not treated as a variational parameter but kept at the value given by the original system,  $\varepsilon' = \varepsilon$ , one would have a finite  $\partial \Omega / \partial \varepsilon'$  in Eq. (12), and the two expressions (6) and (7) for the average particle number would yield different results. This completes the proof.

Equation (6) for the average particle number of the lattice model can be compared with

$$\langle N \rangle' = -\frac{\partial \Omega'}{\partial \mu} = \sum_{i\sigma} \int_{-\infty}^{\infty} f(\omega) A'_{ii\sigma}(\omega) d\omega, \quad (13)$$

which gives the average particle number of the reference system. Again, there are two ways to get  $\langle N \rangle'$ : either as the

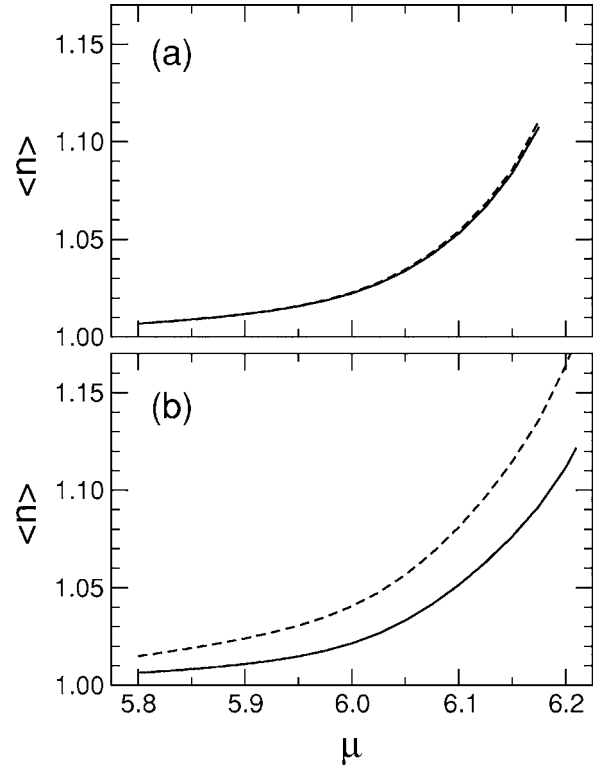


FIG. 1. Filling  $n = \langle n_{i\sigma} \rangle$  as a function of chemical potential  $\mu$  obtained by integration of the spectral density [Eq. (7), solid lines] and via the derivative of  $\Omega$  [Eq. (6), dashed lines]. Results are obtained, respectively, by considering  $\varepsilon'$  as a variational parameter (a) and by setting  $\varepsilon' = 0$  (b). Calculations for the electron-doped case with  $U = 8$ , nearest-neighbor hopping  $t_{nn} = -1$  and next-nearest-neighbor hopping  $t_{nmm} = 0.3$ .

derivative of the reference system's grand potential  $\Omega' \equiv \Omega_{t',U}$  or by frequency integration of the reference system's spectral density  $A'_{ii\sigma}(\omega) \equiv (-1/\pi) \text{Im} G'_{ii\sigma}(\omega + i0^+)$ . As the reference system is solved exactly, both ways must yield the same result. Note, however, that  $\langle N \rangle \neq \langle N \rangle'$  in general.

The above reasoning can straightforwardly be generalized to the off-diagonal ( $i \neq j$ ) elements of the one-particle density matrix  $\langle c_{i\sigma}^\dagger c_{j\sigma} \rangle$ . This is discussed in Appendix A.

The effect of thermodynamic (in)consistency is illustrated for the single-band Hubbard model of Eq. (1) in Fig. 1. The figure shows  $n = \langle n_{i\sigma} \rangle$  as a function of  $\mu$  as obtained from VCA calculations described in Sec. II C below. Solid lines display the result obtained by frequency integration of the spectral density, Eq. (7), while dashed lines show the result of the numerical  $\mu$  derivative of  $\Omega$ , Eq. (6). We compare the results obtained by considering  $\varepsilon'$  as a variational parameter (a), with the ones obtained by setting  $\varepsilon' = 0$  (b). In case (a) the two curves coincide within numerical accuracy, as expected, while in case (b) a considerable discrepancy is observed. This discrepancy increases upon approaching the transition to the nonmagnetic state—i.e., precisely in the interesting region, where it reaches about 5% doping.

While thermodynamic consistency with respect to the particle number is an issue for most approximations within the SFT, there is one exception: the cellular DMFT. This is discussed in Appendix B.

### C. Variational cluster approach

In detail, the calculation proceeds as follows: We consider the 2D single-band Hubbard model of Eq. (1) with nearest- ( $t_{nn}$ ) and next-nearest- ( $t_{nnn}$ ) neighbor hoppings and the Hubbard  $U$ . For the purpose of our qualitative description of the HTSC's, it is sufficient to take parameters which are typical for both hole- and electron-doped high- $T_c$  cuprates—i.e.,  $t_{nnn}/t_{nn} = -0.3$  and  $U/t_{nn} = 8$ . The energy scale is set by choosing  $t_{nn} = -1$ . Different values of the parameters (e.g., a change of  $U$  or  $t_{nnn}$  within  $\sim 30\%$ ) or a third-nearest-neighbor hopping have been also incorporated, checked, and found not to qualitatively change our conclusions (for example, concerning the weak phase separation detected in the electron-doped case).

The Hamiltonian of the reference system  $H'$  is given by a set of decoupled clusters of finite size. For an individual cluster, the Hamiltonian reads

$$H'_{\text{cluster}} = H'_{\text{Hub}} + H'_{\text{AF}} + H'_{\text{SC}}. \quad (14)$$

It consists of the Hubbard Hamiltonian confined to the finite cluster  $H'_{\text{Hub}}$  plus two symmetry-breaking terms (Weiss fields)  $H'_{\text{AF}}$  and  $H'_{\text{SC}}$  with

$$H'_{\text{AF}} = h'_{\text{AF}} \sum_{i\sigma} (n_{i\uparrow} - n_{i\downarrow}) e^{i\mathbf{Q}\cdot\mathbf{R}_i} \quad (15)$$

and

$$H'_{\text{SC}} = h'_{\text{SC}} \sum_{ij} \frac{\eta_{ij}}{2} (c_{i\uparrow} c_{j\downarrow} + \text{H.c.}), \quad (16)$$

where  $h'_{\text{AF}}$  is the strength of the staggered and  $h'_{\text{SC}}$  the strength of the nearest-neighbor  $d$ -wave pairing field.  $\mathbf{Q} = (\pi, \pi)$  is the AF wave vector, and  $\eta_{ij}$  denotes the  $d$ -wave form factor which is nonvanishing for nearest-neighbor lattice sites only and is equal to  $+1$  ( $-1$ ) for  $\mathbf{R}_i - \mathbf{R}_j$  in the  $x$  ( $y$ ) direction. The sum in Eq. (16) is restricted to sites  $i$  and  $j$  belonging to the same cluster. According to the discussion in Sec. II B, the site-independent energy  $\varepsilon' = t'_{ii}$  shall be treated as a variational parameter. It shows up in the local term

$$H'_{\text{local}} = \varepsilon' \sum_{i\sigma} n_{i\sigma}, \quad (17)$$

which is already included in  $H'_{\text{Hub}}$ . The optimization of  $\varepsilon'$  has to be done simultaneously with the optimization of the parameters  $h'_{\text{AF}}$  and  $h'_{\text{SC}}$ .

Due to the optimization of the Weiss field strengths  $h'_{\text{AF}}$  and  $h'_{\text{SC}}$ , one can account for spontaneous AF and  $d$ -wave SC symmetry breaking. The respective AF and SC order parameters  $m$  and  $\Delta$  are defined as

$$m = \frac{\partial \Omega}{\partial h_{\text{AF}}}, \quad \Delta = \frac{\partial \Omega}{\partial h_{\text{SC}}}, \quad (18)$$

in the limit  $h_{\text{AF}}, h_{\text{SC}} \rightarrow 0$  where  $h_{\text{AF}}$  and  $h_{\text{SC}}$  are the strengths of external *physical* staggered and pairing fields. These physical fields should not be confused with the fictitious Weiss fields with strengths  $h'_{\text{AF}}$  and  $h'_{\text{SC}}$ . Adding the respective physical field terms to the Hamiltonian  $H$  and performing the derivative with respect to  $h_{\text{AF}}$  and  $h_{\text{SC}}$  of the SFT

grand potential (at the respective optimal fictitious field strengths  $h'_{\text{AF}}$  and  $h'_{\text{SC}}$ ) yields  $m$  and  $\Delta$  consistently with their representations (on the “one-particle level”) as frequency integrals over the usual and anomalous one-particle spectral density. This consistency is shown in the same way as in Sec. II B for the average particle number and is a consequence of treating the fictitious fields as variational parameters.

The quality of the approximation is decisively influenced by the cluster size used. On the one hand, for an appropriate characterization of the phase transition (as considered in Sec. IV, below), one needs a sufficient accuracy in the grand potential  $\Omega$ . This accuracy is, first of all, determined by the requirement that the clusters chosen must be large enough to fully account for the “short-range” spatial dependence of the self-energy as has been discussed below Eq. (2). On the other hand, for a given cluster size, an as accurate as possible numerical evaluation has to be employed.

With respect to the latter, we found it both convenient and accurate to evaluate the frequency integrals contained in the trace in Eq. (4), not by numerical integration (where the required accuracy is difficult to achieve), but by converting these integrals to a sum over the poles of the Green's function (see Ref. 8 for details). This, however, requires the computation of all many-body eigenstates in a given sector of the cluster Hamiltonian  $H'_{\text{cluster}}$  [Eq. (14)] including symmetry-breaking fields. This technically limits the cluster sizes to be considered. Therefore, in the present work, we have chosen an infinite lattice tiled with  $2 \times 2$  clusters.

Clusters consisting of  $2 \times 2$  sites, as well as larger cluster sizes, have recently been systematically studied by Kyung *et al.*<sup>44</sup> in their influence on various physical quantities of the 2D Hubbard model by means of the C-DMFT. Already the smallest—i.e.,  $2 \times 2$ —cluster has been found to account for more than 95% of the “correlation effect” in the single-particle spectrum [for a precise definition see Eq. (16) of Ref. 44]. This suggests that at least some of the relevant questions in a strongly correlated electron system, modeled by a Hubbard-type Hamiltonian, may be studied, even rather accurately, with a such a small reference cluster.

Nevertheless, for a more accurate determination of the SC state and of the phase transition, larger clusters have to be considered eventually. Only in this way can phase-fluctuation effects between different  $d$ -wave Cooper pairs (which determine the spatial dependence of the self-energy in the SC state) be accounted for. We expect, for example, that calculations for larger clusters would display a smaller SC gap than the one seen in Fig. 4(b), below, around  $(\pi, 0)$  in the electron-doped case. On the other hand, we expect our results on the global phase diagram to be quite robust. This is corroborated by the only weak dependence on (moderate) model changes, such as the next-nearest hopping or the Hubbard interaction.<sup>14,15</sup>

### III. SINGLE-PARTICLE EXCITATIONS

The evolution of the single-particle excitation spectrum  $A(\mathbf{k}, \omega)$  as a function of hole doping and, in particular, the transition from a “small” Fermi surface [hole pockets around  $(\pi/2, \pi/2)$ ] to a local-density-approximation-like (LDA-

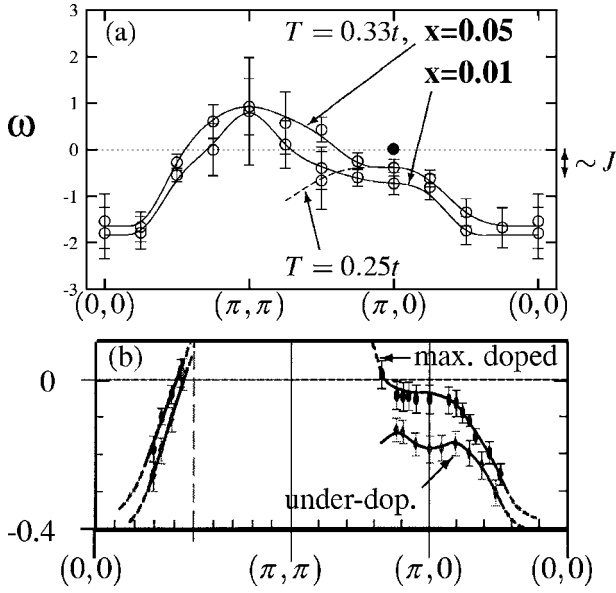


FIG. 2. Taken from Ref. 13. The dispersion of the peaks in the single-particle spectral weight from (a) QMC simulations of the Hubbard model at the temperatures indicated and at dopings  $x=0.01$ ,  $x=0.05$  [peaks in  $A(\mathbf{k}, \omega)$  represented by error bars], and  $x=0.13$  (solid circle). (b) ARPES experiments from underdoped and optimally doped materials [peak centroids in  $A(\mathbf{k}, \omega)$ ], after Ref. 30.

like) Fermi surface closed around  $(\pi, \pi)$  are key observations in unlocking the mystery of the cuprates. Earlier QMC calculations for the 2D Hubbard model<sup>11,13</sup> found that the single-particle spectral weight  $A(\mathbf{k}, \omega)$  semiquantitatively reproduces both the momentum ( $d_{x^2-y^2}$  symmetry) and, in particular, doping dependence of the “high-energy” pseudogap of the order of the exchange energy  $J \sim 200$  meV as found in photoemission experiments around  $(\pi, 0)$ . The corresponding QMC data are reproduced in Fig. 2 for comparison with the results of the VCA shown in Fig. 3 for hole dopings  $x=0.01$  and  $x=0.05$ .

We first discuss the QMC data. In the underdoped regime, the “pseudogap” feature near  $(\pi, 0)$  moves to lower binding energy as doping is increased. At about  $x=0.13$  (solid circles in Fig. 2) the pseudogap vanishes, in overall accordance with the experimental findings.<sup>10</sup> In the experiments, the “high-energy” pseudogap is identified with the centroids of spectral weight near  $(\pi, 0)$ .

However, the experimental ARPES spectra also display a “low-energy” pseudogap in the normal (superconducting) state above (below)  $T_c$  with energy  $\sim 20$  meV, inferred from the leading edge in the spectral density, which also opens up in the underdoped regime and vanishes in the overdoped regime.<sup>10</sup> This empirical correlation between the disappearance of the “high-energy” pseudogap and the decrease of the SC gap and, therefore, pairing strength suggested already several years ago that the high-energy features at  $(\pi, 0)$  (which are correctly described by the “high-temperature” QMC simulations) are closely related to the pairing interaction.<sup>10</sup>

It is clear, however, that there is a strong need to perform calculations at much lower temperatures: i.e., temperatures

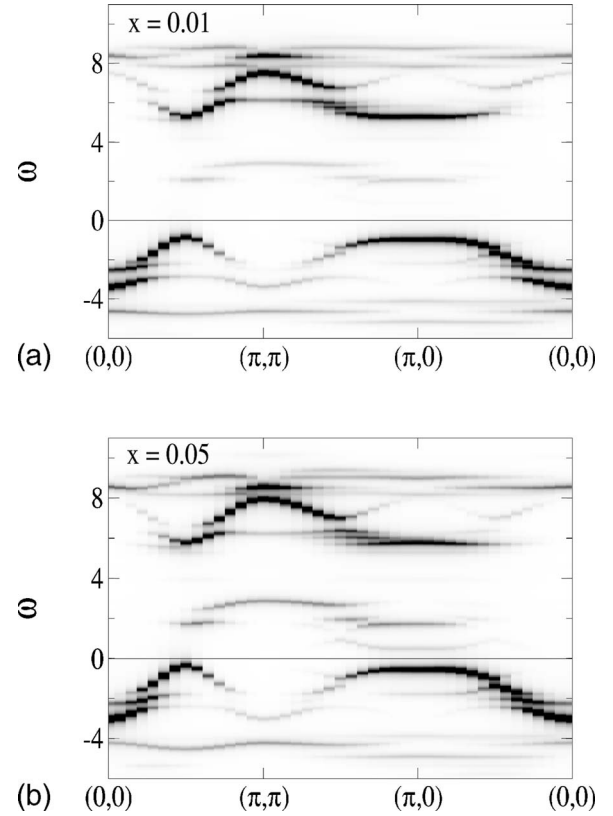


FIG. 3. Single-particle spectrum for the hole-doped ( $x=0.01$  and  $x=0.05$ ) case at  $U=8$  ( $t_{nn}=-1$ ). For comparison with the QMC data, the next-nearest-neighbor hopping is set to  $t_{nm}=0$ .

below  $T_c \sim 20$  meV. Only then can the “low-energy” SC or normal-state pseudogap be detected and only then can the question, “where do holes enter first?” be answered correctly. According to the results of the “high-temperature” ( $T=0.33$ ) QMC simulations shown in Fig. 2 for  $x=0.01$ , holes enter first around  $(\pi, \pi)$ . This can be understood by referring to the idea<sup>12,13</sup> that a higher temperature  $T$  effectively acts as an increased doping which destroys the magnetic Brillouin zone. This allows holes to first enter into the “arc” of single-particle excitations spanned around  $\mathbf{Q} = (\pi, \pi)$ .

However, a portion of the corresponding “large” Fermi surface seems to disappear already at the lower temperature  $T=0.25$ . This is indicated in Fig. 2(a) by the downturn of the quasiparticlelike band between  $(\pi, 0)$  and  $(\pi, \pi)$ . In the experiment [Fig. 2(b)], this behavior in the underdoped regime has been interpreted as the opening of a pseudogap in the underlying Fermi surface near the  $(\pi, 0)$  to  $(\pi, \pi)$  line.<sup>10</sup> This opening is obviously intimately related to the above question: namely, where doped holes first enter—i.e., to the possibility of hole pockets developing at very small temperatures and low dopings around  $(\pi/2, \pi/2)$  in the hole-doped case.

In contrast to the finite- $T$  QMC result, the corresponding VCA calculations for  $T=0$  (see Fig. 3) show that holes first go into the coherent band around  $(\pi/2, \pi/2)$  forming “hole pockets” consistent with experiments.<sup>10</sup> Note that for the dopings considered in Fig. 3, the system is in a mixed AF

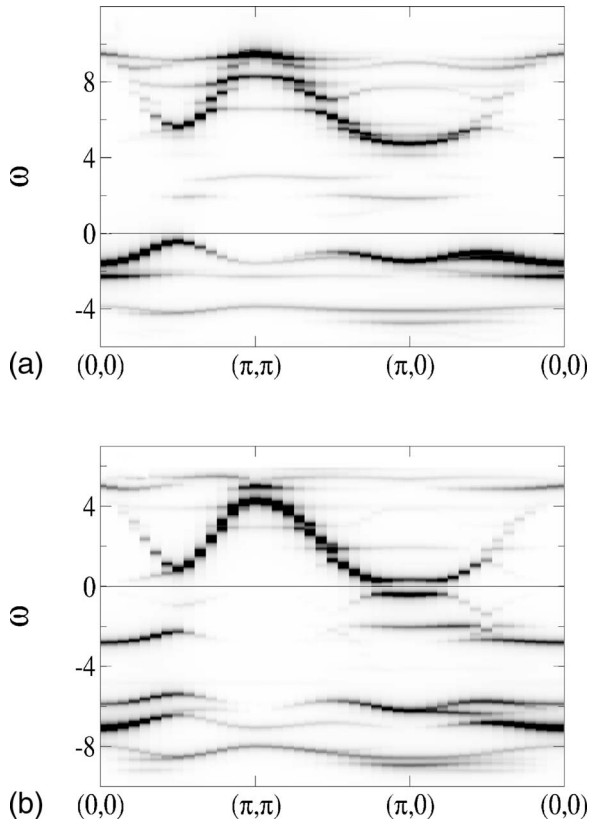


FIG. 4. Single-particle spectrum for  $U=8$  and  $t_{mn}=0.3$  ( $t_{mn}=-1$ ) in the hole-doped (a) and electron-doped (b) cases. Results are shown for dopings in the mixed AF+SC state (see Sec. IV)—i.e., for  $x=0.015$  (a) and  $x=0.09$  (b), respectively.

+SC state with nonvanishing AF order parameter (see also Fig. 7, below). Therefore, although the low-lying spectral weight is found around  $(\pi/2, \pi/2)$ , the spectrum still shows an AF gap at this wave vector.

Related to this, it appears that even for  $x=0.05$  the quasi-particlelike dispersion does not cross the Fermi energy along the nodal direction [between  $(0,0)$  and  $(\pi, \pi)$ ] in contrast to the experimental situation in Fig. 2(b). Although some (weak) accumulation of spectral weight close and above  $\omega=0$  can be seen in Fig. 3, we believe that this noncrossing is (partly) a shortcoming of our  $2 \times 2$  calculation and that the self-energy in the nodal direction requires larger clusters.

To address this issue for more realistic model parameters—i.e., including a next-nearest-neighbor hopping  $t_{mn}=-0.3t_{nn}$ —as well as to study the corresponding doping evolution in the electron-doped case, we discuss the VCA results for  $A(\mathbf{k}, \omega)$  shown in Fig. 4. The calculations have been performed for the hole-doped (a) and for the electron-doped (b) systems in the mixed AF+SC phase (see Sec. IV)—i.e., for  $x=0.015$  and  $x=0.09$ , respectively.

Let us concentrate on the very small (1.5%) hole doping first. In agreement with the corresponding experiments<sup>10</sup> in hole-doped cuprates, holes indeed first enter at  $(\pi/2, \pi/2)$ . Although the system is in a mixed AF+SC phase (see Sec. IV), the SC gap is zero at this nodal point, so that doping into nodal states—i.e., normal metallic screening—apparently destabilizes the AF solution already for rather low doping val-

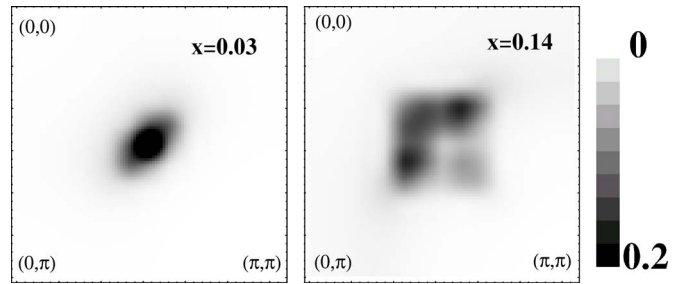


FIG. 5. (Color online) Evolution of the low-energy spectrum upon hole doping. Parameters are as in Fig. 4. The weight is obtained by integrating the low-energy  $A(\mathbf{k}, \omega)$  spectrum down to 0.2 below the Fermi energy.

ues ( $x \sim 0.03$ ). This explains the phase diagram of Fig. 7, below.

A similar picture can be inferred by looking at the evolution of the Fermi surface as a function of doping. This can be extracted from Fig. 5 where the low-energy spectral weight is plotted in the Brillouin zone. In qualitative agreement with experiments, hole pockets start forming around  $(\pi/2, \pi/2)$  for low doping, while a large Fermi surface centered about  $(\pi, \pi)$  starts building up at higher doping.

In contrast, in electron-doped systems, doped electrons initially form pockets around  $(\pi, 0)$  [see Figs. 4(b) and 6; see also Refs. 14 and 31], in agreement with experiments.<sup>32,33</sup> Figure 6 shows the spectral weight obtained by integrating  $A(\mathbf{k}, \omega)$  down to 0.2 below the Fermi energy ( $\omega=0$ ). One has to be careful when interpreting Fig. 6, since for  $x < 0.13$  there is still an AF gap at the Fermi surface near  $(\pi/2, \pi/2)$  besides the SC one near  $(\pi, 0)$ . Therefore, the excitation spectrum is completely gapped, and one has to go away from  $\omega=0$  in order to find some weight. Since we integrate only in a small energy window around the Fermi level, the scale in Fig. 6 is an order of magnitude smaller than in the hole-doped case, Fig. 5, for which the AF gap near  $(\pi/2, \pi/2)$  is shifted away from the Fermi surface. Nevertheless, one finds that the lowest-lying states in the electron-doped case are around  $(\pi, 0)$ . Here, the density of states is large and pro-

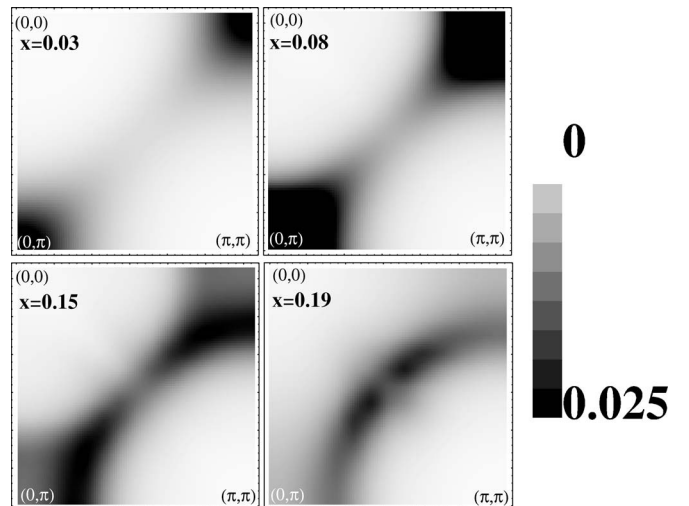


FIG. 6. The same as in Fig. 5 but for the electron-doped case.

vides a large “reservoir” for electron doping. This, in combination with the fact that the chemical potential lies in the SC gap (of the AF+SC phase), stabilizes the AF solution for a larger doping range than in the hole-doped case, allowing for the AF gap to decrease more gradually (see Sec. IV). Also in this case, the breakdown of the magnetic solution occurs as soon as the chemical potential reaches the bottom of the band at  $(\pi/2, \pi/2)$ . The observation that doping into  $(\pi/2, \pi/2)$  generically makes the AF phase unstable suggests that also the occurrence of phase separation, to be discussed in Sec. IV, is rather generic and quite independent of model details.

The low-energy spectral weight, as plotted for different dopings in Fig. 6, agrees quite well with the ARPES measurements of Armitage *et al.*,<sup>32,33</sup> doped electrons away from half-filling first form pockets around  $(\pi, 0)$ . At higher doping, Fermi-surface segments start developing along the  $(\pi, 0)$ - $(0, \pi)$  line. Finally, these segments connect and form a large Fermi surface around  $(\pi, \pi)$  near optimal doping.

#### IV. GROUND-STATE PHASE DIAGRAM

In this section the ground-state phase diagram and the AF to SC transition are presented and discussed (see also Refs. 14 and 15). In particular, we will focus on the similarities and differences between the hole- and electron-doped systems as well as their relation with the evolution of the single-particle spectrum.

In order to determine the  $T=0$  phase diagram, we proceed as described in Sec. II C; i.e., two symmetry-breaking terms (Weiss fields)  $H'_{AF}$  and  $H'_{SC}$  are included and their respective strengths  $h'_{AF}$  and  $h'_{SC}$  are treated as variational parameters in addition to  $\varepsilon'$ . As discussed in Sec. II B, the use of the additional variational parameter  $\varepsilon'$  is required in order to have a consistent determination of the particle density.

The phase diagram for the Hubbard model with  $U=8$  and next-nearest-neighbor hopping  $t_{nm}=0.3$  (we set  $t_{nn}=-1$ ), as obtained from our calculations, is shown in Fig. 7 for the hole-doped and in Fig. 8 for the electron-doped case. In the upper part of each figure, the chemical potential  $\mu$  is plotted as a function of  $x$ . In the corresponding lower parts, we display the AF ( $m$ ) and SC ( $\Delta$ ) order parameter as a function of doping  $x$ . Note that the order parameters  $m$  and  $\Delta$  are different from the Weiss fields  $h'_{AF}$  and  $h'_{SC}$ , respectively. Quite generally, however, a nonvanishing stationary value for a Weiss field produces a nonvanishing order parameter, respectively, although the latter can be much smaller.

Let us discuss hole doping first (see Fig. 7). For low dopings  $x$  we find a homogeneous symmetry-broken phase in which both the AF as well as the SC order parameter  $m$  and  $\Delta$  are nonzero. This corresponds to a phase where AF and SC order microscopically and coherently coexist. A homogeneous phase with pure SC ( $m=0$  and  $\Delta>0$ ) is obtained for larger dopings. The behavior of  $m$  vs  $x$  in Fig. 7 seems to suggest that the transition to the nonmagnetic state is continuous (second order) as a function of doping. However, a glance at the nonmonotonous behavior of the chemical potential  $\mu$ , plotted as a function of  $x$  in the upper part of the figure, indicates the occurrence of a charge instability. The

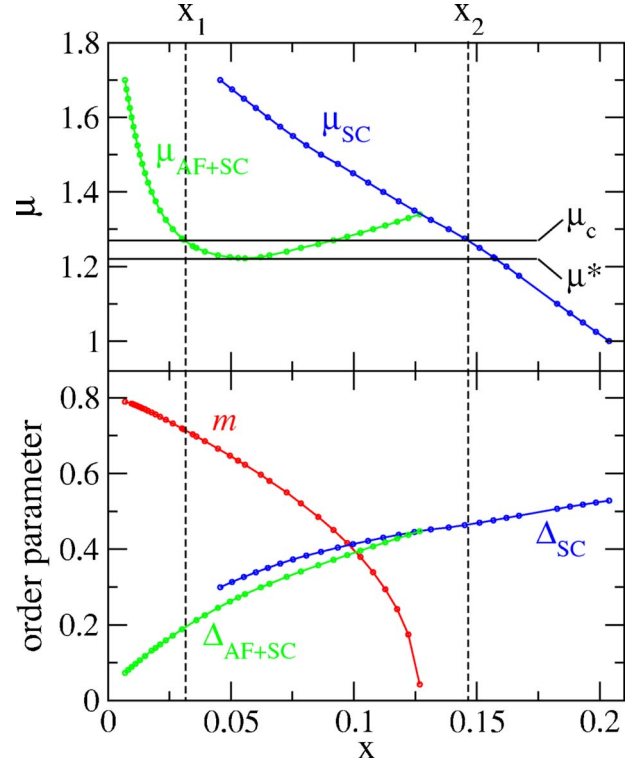


FIG. 7. (Color online) Antiferromagnetic and superconducting order parameters  $m$  and  $\Delta$  and chemical potential  $\mu$  as functions of hole doping  $x$ .  $\Delta$  and  $\mu$  are plotted for the AF+SC (green,  $\Delta_{AF+SC}$ ,  $\mu_{AF+SC}$ ) as well as for the pure SC homogeneous solutions (blue,  $\Delta_{SC}$ ,  $\mu_{SC}$ ). Note that  $\Delta$  is scaled by a factor of 5 for convenience. For  $x < x_1$  the system exhibits a coexistence of AF and  $d$ -wave SC order. Phase separation occurs between the doping levels  $x_1$  and  $x_2$ . For  $x > x_2$  pure  $d$ -wave SC is realized. In the phase separation region  $x_1 < x < x_2$ , the homogeneous solution becomes unstable and the system prefers to separate into a mixture of two densities corresponding to  $x_1$  and  $x_2$ . The chemical potential  $\mu_c$  is determined by the Maxwell construction shown in the upper figure. At  $\mu^*$  the slope of the AF+SC solution changes sign.

system tends to separate into a hole-poor ( $x_1$ ) and a hole-rich ( $x_2$ ) phase. The two dopings  $x_1$  and  $x_2$ , as well as the chemical potential  $\mu_c$  in the phase-separated region, are identified by the Maxwell construction shown in the upper part of Fig. 7. Here  $\mu^*$  is the point where the slope of  $\mu(x)$  changes sign.

Of course, this phase separation is obtained within a treatment that, in the present work, just considers for homogeneous order parameters only and that neglects surface effects. Furthermore, the VCA is a mean-field-type approach to length scales beyond the size of the individual cluster. Therefore, the above result has to be interpreted with care. We expect it to signal a *tendency* towards the formation of microscopic inhomogeneities, such as stripes, checkerboard patterns, etc.<sup>34,35,37</sup> This tendency will be further studied in future work by considering larger clusters and/or by allowing for a more general variational solution which explicitly describes stripe inhomogeneities (for example, by considering coupled clusters with different dopings, as in Ref. 36). In this case, one might expect the phase transition to become more continuous and phase separation to disappear eventually.

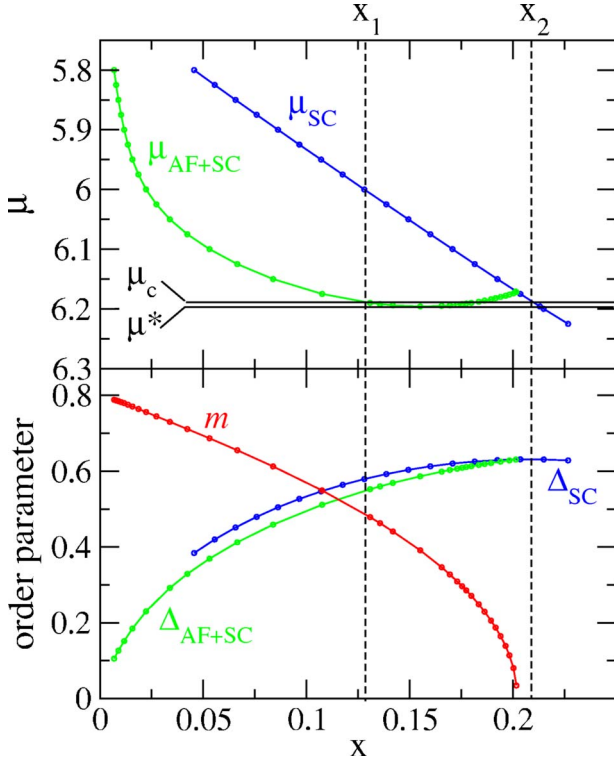


FIG. 8. (Color online) Same as Fig. 7 but for electron doping. Note the enhanced robustness of the AF state and the strongly reduced scale  $\Delta\mu \equiv (\mu^* - \mu_c)$  as compared to hole doping.

Let us now discuss the electron-doped case and the similarities and differences as compared to hole doping. The first observation is that, while the phase diagrams in Figs. 7 and 8 are *qualitatively* similar, the phase in which long-range AF order is realized is spreading to significantly larger doping values in the electron-doped case, in overall agreement with the experimental situation. Figure 8 shows that phase separation occurs in the electron-doped case as well, although the associated energy scale  $\Delta\mu \equiv (\mu^* - \mu_c)$  is smaller with respect to the hole-doped case by about an order of magnitude. In Ref. 15 it is argued that this can be related to the different pseudogap and SC transition scales in hole- and electron-doped materials. This may give support to theories<sup>34,38</sup> which are based on the notion that fluctuations of competing phases, or of the related order parameters, are responsible for the pseudogap phenomenon.

Depending on the value of  $\mu$ , there may be two solutions—an AF+SC and a pure SC one—corresponding to two stationary points of  $\Omega$ . In order to gain insight into the first-order transition between these two solutions, it is instructive to observe the behavior of the grand potential  $\Omega$  as a function of the variational parameter  $h'_{AF}$  associated with this transition for different  $\mu$ . For simplicity, we consider here the hole-doped case only. Results are plotted in Fig. 9. Note that  $h'_{AF}$  is varied, while the other two variational parameters  $h'_{SC}$  and  $\varepsilon'$  are fixed at their values at the respective stationary point. At low doping, there is a single minimum of the grand potential  $\Omega$  at a finite value  $h'_{AF}$  only (Fig. 9,  $\mu = 1.35$ ). In contrast, the paramagnetic ( $h'_{AF} = 0$ ) solution is given by a local maximum. Upon further doping,  $\Omega$  *addition-*

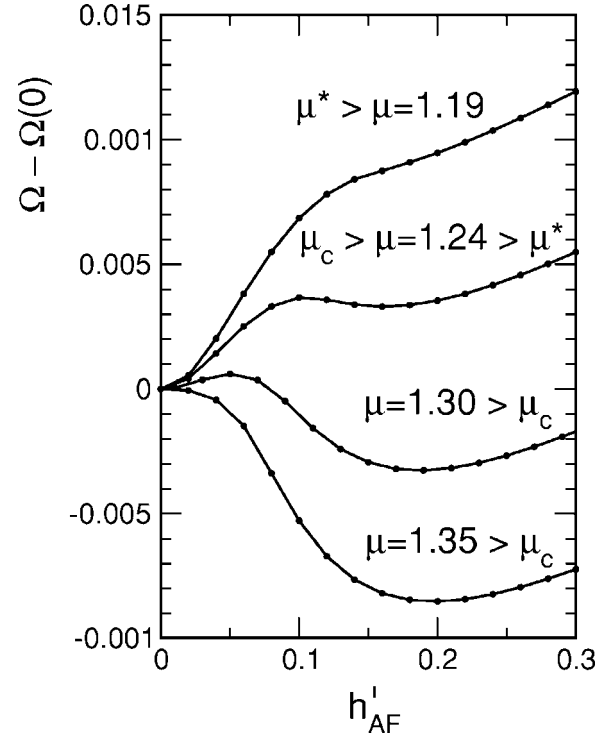


FIG. 9.  $\Omega$  vs  $h'_{AF}$  (with the two other parameters  $h'_{SC}$  and  $\varepsilon'$  fixed at their stationary-point values) for different  $\mu$  in the hole-doped case. Parameters:  $U=8$  and  $t_{mn}=0.3$  ( $t_{nn}=-1$ ).

*ally* develops a local minimum at vanishing AF variational parameter  $h'_{AF}=0$  (Fig. 9,  $\mu=1.30$ ). For  $\mu < \mu_c$ , the minimum at  $h'_{AF}=0$  becomes lower than the one at finite  $h'_{AF}$  indicating a first-order phase transition to a nonmagnetic state (Fig. 9,  $\mu=1.24$ ). Eventually, the local maximum lying between the two minima merges with the minimum at finite  $h'_{AF}$  and the AF solution disappears (Fig. 9,  $\mu=1.19$ ). This disappearance just occurs when the chemical potential  $\mu$  enters the quasiparticle band around  $(\pi/2, \pi/2)$  ( $\mu^* = 1.22$ ).

Although Fig. 9 displays the results for the hole-doped case, this behavior occurs qualitatively in the electron-doped case as well, although with a much smaller characteristic energy scale as discussed above. Again, these results reflect a qualitatively similar behavior for electron and hole doping.

## V. SUMMARY AND CONCLUSIONS

By means of a recently developed quantum-cluster approach, we have carried out a detailed analysis of the phase transition from the antiferromagnetic to the superconducting phase in the Hubbard model at zero temperature. The main results concerning the nature of the AF to SC transition are summarized in Figs. 7 and 8. At low dopings the AF phase actually mixes with a weak *d*-wave SC component. A similar coexistence phase is observed—for example, in PrCeCuO (Ref. 39)—and was also obtained in previous mean-field and cluster calculations.<sup>14,38,40</sup> Upon further increasing doping, we find a transition to a pure *d*-wave SC phase.

The phase-separation scenario, which is found for hole but also for electron doping within our approximation,

should carefully be interpreted as a general *tendency* of the system to form microscopically inhomogeneous phases. Indeed, by allowing for a more general spatial dependence of the order parameter, the macroscopic phase separation will probably be replaced by other microscopically inhomogeneous phases, such as stripes, checkerboard order, etc. In particular, this might be expected to be the case if the long-range Coulomb interaction is taken into account additionally.<sup>34,41,42</sup> The situation is subtle in the electron-doped case. Here, in contrast to previous theoretical calculations, our results also suggest phase separation, although the corresponding energy scale (see Fig. 8) is one order of magnitude smaller than in hole-doped compounds.

Our results for the single-particle excitations presented in Sec. III support the idea that it is, in fact, the single-particle spectrum which holds the key for understanding the qualitative differences seen in the ground-state phase diagram between the hole- and electron-doped cuprates. This concerns, for example, the robustness of the AF state in the electron-doped case. Here, electrons initially form pockets around  $(\pi, 0)$  in accordance with experiments.<sup>32</sup> The fact that the density of states is large there, as well as the presence of a SC “gap” at this nodal point, stabilizes the AF state for a larger doping regime as compared to the hole-doped case. The breakdown of the magnetic solution appears as soon as “normal” metallic screening sets in—i.e., when  $\mu$  touches the band at  $(\pi/2, \pi/2)$ .<sup>15</sup>

One should note that the variational cluster approach is able to treat the fluctuations correctly up to the range of the cluster size only. Therefore, the question arises whether the SC solution we (and also others<sup>14,40,43</sup>) obtain within the AF phase is a true long-range SC phase or whether it is only a signal of strong pairing fluctuations within the AF phase leading to a SC pseudogap. The latter hypothesis could be supported by the fact that results obtained with different cluster sizes<sup>14</sup> seem to indicate a size dependence of the SC order parameter and by the fact that the SC order parameter is about a factor of 3 smaller in the AF+SC phase than in the pure SC one. The presence or not of such a microscopic coexistence phase may depend on material details. Certainly, our results suggest that the SC gap  $\Delta$  (or pseudogap in the case of fluctuations) is important in order to stabilize the AF phase in electron-doped materials, as discussed in Sec. III.

Similar VCA calculations have recently been carried out by Sénéchal *et al.*<sup>14</sup> using clusters up to 10 sites but without the variation of the on-site energies. These authors show that the single-band Hubbard model is sufficient to explain the different overall shapes of the phase diagrams for hole- and electron-doped cuprates. However, their results seem to suggest that in the electron-doped case the AF to SC transition is continuous and associated with a quantum-critical point, in contrast to our results. This clearly shows the importance for a consistent determination of the average particle number.

The recent substantial progress in relating the “high-energy” physics of the Hubbard model and its variants to the low-energy physics of competing phases is to a large extent due to the development of different quantum-cluster theories. Apart from the VCA, these are the cluster extensions of the DMFT, such as the C-DMFT and DCA. Kyung *et al.*<sup>44</sup> have shown that some of the important problems in

strongly correlated electron systems may be studied highly accurately using comparatively small clusters. Maier and co-workers<sup>21,22</sup> performed a systematic cluster-size study of the 2D Hubbard model using rather large clusters (up to 26 sites). Converged results suggest a finite- $T$  instability to  $d$ -wave SC state. Because of the QMC minus-sign problem, however, results were limited to  $U=4t$  where the typical correlation energy  $U$  and the magnetic energy scale of the HTSC is not yet achieved. On the other hand, the present VCA studies are clearly not yet converged with respect to the cluster size, as one can read off from, for example, the relatively large SC gap in the single-particle excitations, displayed in Fig. 5. An extension to larger clusters is, at least in principle, also possible within the VCA. This, however, necessarily implies the use of stochastic (QMC) methods as solvers for the cluster reference system.

### ACKNOWLEDGMENTS

We would like to thank D. J. Scalapino for many useful discussions. One of us (W.H.) would additionally like to acknowledge the hospitality of the Kavli Institute for Theoretical Physics in Santa Barbara (supported by NSF Grant No. PHY99-0794). The work was supported by the DFG Forschergruppe 538, by the KONWIHR supercomputing network in Bavaria, and by FWF Project No. P18505-N16.

### APPENDIX A: ONE-PARTICLE DENSITY MATRIX

The reasoning in Sec. II B can straightforwardly be generalized to the off-diagonal ( $i \neq j$ ) elements of the one-particle density matrix  $\langle c_{i\sigma}^\dagger c_{j\sigma} \rangle$ . In this case, thermodynamic consistency means that, for a selected pair of sites  $(i, j)$ , the derivative

$$\langle c_{i\sigma}^\dagger c_{j\sigma} \rangle = \frac{\partial \Omega}{\partial t_{ij\sigma}} \quad (\text{A1})$$

is equivalent to the integral

$$\langle c_{i\sigma}^\dagger c_{j\sigma} \rangle = \int_{-\infty}^{\infty} f(\omega) A_{ji\sigma}(\omega) d\omega, \quad (\text{A2})$$

where, for convenience, the hopping is formally assumed to be spin dependent.

Starting with Eq. (A1), we note that the  $t_{ij\sigma}$  dependence of  $\Omega \equiv \Omega_{t,U}[\sum_s t'_s, U]$  is due to the explicit  $t_{ij\sigma}$  dependence of the free Green’s function  $G_{0,t}$  in Eq. (4) and due to the implicit  $t_{ij\sigma}$  dependence of  $t'_s$ :

$$\begin{aligned} \langle c_{i\sigma}^\dagger c_{j\sigma} \rangle &= \frac{\partial \Omega_{t,U}[\sum_s t'_s, U]}{\partial t_{ij\sigma}} \\ &= T \sum_{\omega_n} e^{i\omega_n 0^+} \left( \frac{1}{G_{0,t}^{-1}(i\omega_n) - \sum_s t'_s U(i\omega_n)} \right)_{ji\sigma} \\ &\quad + \left. \frac{\partial \Omega_{t,U}[\sum_s t'_s, U]}{\partial t'} \right|_{t'=t'_s} \cdot \frac{\partial t'_s}{\partial t_{ij\sigma}}. \end{aligned} \quad (\text{A3})$$

Because of the stationarity of the grand potential, the second

term on the right-hand side (RHS) can be ignored. We are thus left with the first term which, after transforming the Matsubara sum into an integration over real frequencies, exactly yields the desired expression (A2).

In the case that not all elements of  $\mathbf{t}'$  are treated as variational parameters, the derivative of  $\Omega$  in the second term on the RHS is a derivative with respect to those elements only. If, for the given pair of sites  $i$  and  $j$ ,  $t'_{ij\sigma}$  is selected as a variational parameter, the contribution due to the implicit  $t_{ij\sigma}$  dependence vanishes again. If, on the other hand,  $t'_{ij\sigma}$  is not treated as a variational parameter but fixed at  $t'_{ij\sigma}=t_{ij\sigma}$  from the beginning, the second term will give a finite contribution which spoils the thermodynamic consistency.

## APPENDIX B: CELLULAR DMFT

The C-DMFT is obtained by choosing as a reference system disconnected clusters with a continuous noninteracting bath coupled to each cluster site. Carrying out the  $\mathbf{t}'$  partial derivatives in Eq. (5) and using Eq. (4) for the SFT grand potential, we get the Euler equation in the form

$$T \sum_n \sum_{ij\sigma} \left( \frac{1}{\mathbf{G}_{0,t}^{-1} - \Sigma_{t',U}} - \mathbf{G}_{t',U} \right)_{jj\sigma} \frac{\partial \Sigma_{ij\sigma}}{\partial t'} = 0. \quad (\text{B1})$$

Here  $i$  and  $j$  run over the sites of the original lattice, excluding bath sites. The one-particle bath parameters—namely, the on-site energies of the bath sites and the hybridization of the bath sites with the correlated (physical) sites—have to be treated as (a continuous set of) variational parameters. In the C-DMFT it is assumed that bath parameters can be found such that the first factor Eq. (B1) vanishes,

$$\left( \frac{1}{\mathbf{G}_{0,t}^{-1} - \Sigma_{t',U}} \right)_{ij\sigma}(\omega) = (\mathbf{G}_{t',U})_{ij\sigma}(\omega), \quad (\text{B2})$$

for arbitrary  $\omega$  and for sites  $i$  and  $j$  belonging to the same cluster. Note that, by construction of the reference system,  $\Sigma_{ij\sigma}(\omega)$  and also  $\partial \Sigma_{ij\sigma}(\omega) / \partial t'$  vanish if  $i$  and  $j$  belong to different clusters. Consequently, if bath parameters can be found such that Eq. (B2) holds, the Euler equation (B1) will be satisfied, too: The self-energy functional is stationary at

the C-DMFT self-energy. Equation (B2) is just the self-consistency equation of the C-DMFT (see Refs. 6 and 18).

It is easy to see that  $\langle N \rangle = \langle N \rangle'$  within the C-DMFT: This simply follows by comparing Eqs. (12) and (13) for  $\langle N \rangle$  and  $\langle N \rangle'$  and by using the C-DMFT self-consistency equation (B2).

Consider now the high-frequency expansions of the Green's function and of the self-energy of the reference system. Using  $\mathbf{G}' \equiv \mathbf{G}_{t',U}$ ,  $\Sigma \equiv \Sigma_{t',U}$ , and  $\mathbf{G}_0 \equiv \mathbf{G}_{0,t}$  for short, we have (see Ref. 45 for high-frequency expansions in the Hubbard model)

$$G'_{ij\sigma}(\omega) = \frac{\delta_{ij}}{\omega} + \frac{t'_{ij} - \mu \delta_{ij} + U \langle n_{i-\sigma} \rangle' \delta_{ij}}{\omega^2} + \mathcal{O}(\omega^{-3}),$$

$$\Sigma_{ij\sigma}(\omega) = U \langle n_{i-\sigma} \rangle' \delta_{ij} + \mathcal{O}(\omega^{-1}). \quad (\text{B3})$$

Here,  $\langle n_{i-\sigma} \rangle'$  is the average occupation in the reference system. Using  $G_{0,ij\sigma}^{-1}(\omega) = (\omega + \mu) \delta_{ij} - t_{ij}$ , inserting the expansions into the C-DMFT self-consistency equation (B2), and expanding in powers of  $\omega^{-1}$  once more, we immediately find

$$t'_{ij} = t_{ij} \quad (\text{B4})$$

for (correlated) sites  $i$  and  $j$  within the same cluster, and, in particular,  $\varepsilon' = \varepsilon$  where  $\varepsilon' = t'_{ii}$  and  $\varepsilon = t_{ii}$ . This means that, within the C-DMFT, consistency with respect to the particle number is assured by setting the on-site energies within a cluster of the reference system to their “physical” values.

It goes without saying that a consistent determination of  $\langle N \rangle$  requires an *exact* solution of the reference system which, in the case of the C-DMFT, is by no means trivial. An obvious idea is to replace the continuous bath by a few uncorrelated sites only to allow for an application of the Lanczos method (see Ref. 46, for an example). This, however, immediately implies that the self-consistency equation (B2) cannot be fulfilled exactly any longer and, strictly speaking, the determination of the particle number becomes inconsistent *unless*  $\varepsilon'$  is treated as a variational parameter within the SFT framework.

<sup>1</sup>M. Imada, A. Fujimori, and Y. Tokura, Rev. Mod. Phys. **70**, 1039 (1998).

<sup>2</sup>See, for example, S. A. Kivelson *et al.*, Rev. Mod. Phys. **75**, 1201 (2003), as well as Ref. 34.

<sup>3</sup>T. Maier, M. Jarrell, T. Pruschke, and M. H. Hettler, Rev. Mod. Phys. **77**, 1027 (2005).

<sup>4</sup>A. M. S. Tremblay, B. Kyung, and D. Sénéchal, Fiz. Nizk. Temp. **32**, 561 (2006).

<sup>5</sup>W. Hanke, M. Aichhorn, E. Arrigoni, and M. Potthoff, Physica B **378–389**, 60 (2006)

<sup>6</sup>M. Potthoff, M. Aichhorn, and C. Dahnken, Phys. Rev. Lett. **91**, 206402 (2003).

<sup>7</sup>C. Dahnken, M. Aichhorn, W. Hanke, E. Arrigoni, and M. Pott-

thoff, Phys. Rev. B **70**, 245110 (2004); C. Dahnken, M. Potthoff, E. Arrigoni, and W. Hanke, Fiz. Nizk. Temp. **32**, 602 (2006).

<sup>8</sup>M. Potthoff, Eur. Phys. J. B **32**, 429 (2003); **36**, 335 (2003).

<sup>9</sup>See, for example, A. Paramekanti, M. Randeria, and N. Trivedi, Phys. Rev. B **70**, 054504 (2004).

<sup>10</sup>See, e.g., A. Damascelli, Z. Hussain, and Z. X. Shen, Rev. Mod. Phys. **75**, 473 (2004).

<sup>11</sup>P. W. Anderson, Science **235**, 1196 (1987). See also D. J. Scalapino, Phys. Rep. **250**, 330 (1995).

<sup>12</sup>R. Preuss, W. Hanke, and W. von der Linden, Phys. Rev. Lett. **75**, 1344 (1995).

<sup>13</sup>R. Preuss, W. Hanke, C. Gröber, and H. G. Evertz, Phys. Rev.

- Lett. **79**, 1122 (1997).
- <sup>14</sup>David Sénéchal, P. L. Lavertu, M. A. Marois, and A. M. S. Tremblay, Phys. Rev. Lett. **94**, 156404 (2005).
- <sup>15</sup>M. Aichhorn and E. Arrighoni, Europhys. Lett. **71**, 117 (2005).
- <sup>16</sup>W. Metzner and D. Vollhardt, Phys. Rev. Lett. **62**, 324 (1989).
- <sup>17</sup>A. Georges, G. Kotliar, W. Krauth, and M. J. Rozenberg, Rev. Mod. Phys. **68**, 13 (1996).
- <sup>18</sup>G. Kotliar, S. Y. Savrasov, G. Pálsson, and G. Biroli, Phys. Rev. Lett. **87**, 186401 (2001). See also Ref. 40.
- <sup>19</sup>M. H. Hettler, A. N. Tahvildar-Zadeh, M. Jarrell, T. Pruschke, and H. R. Krishnamurthy, Phys. Rev. B **58**, R7475 (1998).
- <sup>20</sup>W. Koller and N. Dupuis, cond-mat/0511294 (unpublished).
- <sup>21</sup>T. A. Maier, M. Jarrell, T. C. Schulthess, P. R. C. Kent, and J. B. White, Phys. Rev. Lett. **95**, 237001 (2005).
- <sup>22</sup>A. Macridin, M. Jarrell, and Th. Maier, cond-mat/0506148 (unpublished).
- <sup>23</sup>J. M. Luttinger and J. C. Ward, Phys. Rev. **118**, 1417 (1960).
- <sup>24</sup>See, for example, W. Hanke and L. J. Sham, Phys. Rev. B **38**, 13361 (1988).
- <sup>25</sup>E. Müller-Hartmann, Z. Phys. B: Condens. Matter **74**, 507 (1989).
- <sup>26</sup>H. Schweitzer and G. Czycholl, Z. Phys. B: Condens. Matter **83**, 93 (1991).
- <sup>27</sup>M. Potthoff, Adv. Solid State Phys. **45**, 135 (2005).
- <sup>28</sup>C. Gros and R. Valenti, Phys. Rev. B **48**, 418 (1993).
- <sup>29</sup>D. Sénéchal, D. Perez, and M. Pioro-Ladriere, Phys. Rev. Lett. **84**, 522 (2000).
- <sup>30</sup>D. S. Marshall *et al.*, Phys. Rev. Lett. **76**, 4841 (1996).
- <sup>31</sup>C. Kusko, R. S. Markiewicz, M. Lindroos, and A. Bansil, Phys. Rev. B **66**, 140513(R) (2002).
- <sup>32</sup>N. P. Armitage, F. Ronning, D. H. Lu, C. Kim, A. Damascelli, K. M. Shen, D. L. Feng, H. Eisaki, Z.-X. Shen, P. K. Mang, N. Kaneko, M. Greven, Y. Onose, Y. Taguchi, and Y. Tokura, Phys. Rev. Lett. **88**, 257001 (2002).
- <sup>33</sup>N. P. Armitage, D. H. Lu, C. Kim, A. Damascelli, K. M. Shen, F. Ronning, D. L. Feng, P. Bogdanov, Z. X. Shen, Y. Onose, Y. Taguchi, Y. Tokura, P. K. Mang, N. Kaneko, and M. Greven, Phys. Rev. Lett. **87**, 147003 (2001).
- <sup>34</sup>E. W. Carlson, V. J. Emery, S. A. Kivelson, and D. Orgad, *Concepts in High Temperature Superconductivity* (Springer-Verlag, Berlin, 2003), Vol. I.
- <sup>35</sup>E. Arrighoni and S. A. Kivelson, Phys. Rev. B **68**, 180503(R) (2003).
- <sup>36</sup>M. G. Zacher, R. Eder, E. Arrighoni, and W. Hanke, Phys. Rev. Lett. **85**, 2585 (2000).
- <sup>37</sup>E. Arrighoni, E. Fradkin, and S. A. Kivelson, Phys. Rev. B **69**, 214519 (2004).
- <sup>38</sup>M. Inui, S. Doniach, P. J. Hirschfeld, and A. E. Ruckenstein, Phys. Rev. B **37**, R2320 (1988).
- <sup>39</sup>Pengcheng Dai, H. J. Kang, H. A. Mook, M. Matsuura, J. W. Lynn, Y. Kurita, Seiki Komiyama, and Yoichi Ando, Phys. Rev. B **71**, 100502(R) (2005).
- <sup>40</sup>A. I. Lichtenstein and M. I. Katsnelson, Phys. Rev. B **62**, R9283 (2000).
- <sup>41</sup>U. Löw, V. J. Emery, K. Fabricius, and S. A. Kivelson, Phys. Rev. Lett. **72**, 1918 (1994).
- <sup>42</sup>E. Arrighoni, A. P. Harju, W. Hanke, B. Brendel, and S. A. Kivelson, Phys. Rev. B **65**, 134503 (2002).
- <sup>43</sup>G. J. Chen, R. Joynt, F. C. Zhang, and C. Gros, Phys. Rev. B **42**, 2662 (1990).
- <sup>44</sup>B. Kyung, G. Kotliar, and A.-M. S. Tremblay, Phys. Rev. B **73**, 205106 (2006).
- <sup>45</sup>M. Potthoff, T. Herrman, T. Wegner, and W. Nolting, Phys. Status Solidi B **210**, 199 (1998).
- <sup>46</sup>S. S. Kancharla, M. Civelli, M. Carbone, B. Kyung, D. Sénéchal, G. Kotliar, and A.-M. S. Tremblay, cond-mat/0508205 (unpublished).